Orbital: The Electronic Journal of Chemistry
journal homepage: www.orbital.ufms.br
e-ISSN 1984-6428

| Vol 11 | | No. 3 | | April-June 2019 |

FULL PAPER

Structural and Mechanistic Studies of γ-Fe_2O_3 Nanoparticle as Hydroxyurea Drug Nanocarrier

Sadaf Avarand, Ali Morsali*, Mohammad Moemen Heravi, and Safar Ali Beyramabadi

Department of Chemistry, Mashhad Branch, Islamic Azad University, Mashhad, Iran & Research Center for Animal Development Applied Biology, Mashhad Branch, Islamic Azad University, Mashhad 917568, Iran.

Article history: Received: 25 November 2018; revised: 27 March 2019; accepted: 30 June 2019. Available online: 01 July 2019. DOI: http://dx.doi.org/10.17807/orbital.v11i3.1367

Abstract:

In this study, the noncovalent interactions and four mechanisms of covalent functionalization of hydroxyurea have been examined using the density functional theory. Quantum molecular descriptors were also studied in noncovalent interactions. Hydroxyurea is an anticancer drug that, when loaded onto the γ-Fe_2O_3 nanoparticles, will have additional properties and efficacy in the medical applications. The Lumo-Homo energy gap of hydroxyurea is greater than that of noncovalent configurations, indicating the high reactivity of hydroxyurea. Hydroxyurea can bond to the γ-Fe_2O_3 nanoparticles through various functional groups such as the CO (k_1 mechanism), the NH_2 (k_2 mechanism), the OH (k_3 mechanism) and the NH (k_4 mechanism). These reactions were considered to calculate the activation energies, the activation enthalpies and the activation Gibbs free energies. Using these calculations, the product of k_4 mechanism was found to be a thermodynamic and kinetic product. These results can be applied to other similar medications.

Keywords: γ-Fe2O3 nanoparticles; hydroxyurea; density functional theory; noncovalent and covalent functionalization; mechanism

1. Introduction

Magnetic nanoparticles (MNPs) are a class of nanoparticles that can be manipulated using magnetic fields. They usually consist of two components: a magnetic material, often iron, nickel, cobalt and their oxides, and a chemical component that has functionality [1-4]. The physical and chemical properties of magnetic nanomaterials (1-100 nm) are based on the chemical structure and synthesis method [5]. The high surface to volume ratio offers the possibility to functionalize different molecules, including the therapeutic agents [6]. Magnetic nanoparticles can be used as a convenient means to deliver the therapeutic agents to the disease site. It also reduces the dosage and side effects of non-specific absorption of cytotoxic drugs by healthy tissues. MNPs can also be used as magnetic targeted carriers (MTC) in early clinical trials, to demonstrate some success with this technique that has been satisfactory for patients [7, 8].

The magnetic properties of nanoparticles are advantageous for many applications in the field of drug delivery, diagnosis and treatment of diseases [9]. If magnetic fields are applied, these particles can be used as drug carriers to deliver therapeutic agents externally to cancerous tumors [10-13]. When drug carriers reach the target point, the drug is released by enzymatic activity or by changes in pH, temperature and osmotic condition [14, 15]. The two main forms of iron oxide nanoparticles (Fe_3O_4 and γ-Fe_2O_3) have been of great interest because of their excellent magnetic properties and their possible uses. Magnetite (Fe_3O_4) and maghemite (γ-Fe_2O_3) are biologically and environmentally friendly and they are potentially non-toxic to the human body.

*Corresponding author. E-mail: almorsali@yahoo.com

These materials can easily decompose, and this property plays an important role in drug delivery. They can also reduce the amount of drug used in the treatment process and minimize the side effects of the drug [3, 16-20].

Hydroxyurea, with its inhibitory effect, can reduce the synthesis of DNA and can therefore lead to cell death [21]. Hydroxycarbamide or hydroxyurea is a chemotherapy drug used to treat many diseases, including sickle cell disease, melanoma, ovariantumor, squamous cell carcinoma of the head and neck, renal carcinoma, chronic myelogenous leukemia, prostate carcinoma and carcinoma of the uterine cervix [22] chronic myeloid leukemia, cervical cancer and polycythemia vera.

Carrier-mediated drug delivery system based on MNPs has emerged as a powerful methodology for the treatment of various pathologies. Therefore, molecular models are needed to understand the mechanism of functionalization of the drug onto nanoparticles in solvents, especially water [23, 24]. Quantum computations can be very effective in designing and evaluating drug delivery systems. As the 2016 Nobel laureates in chemistry showed, the molecular machines could be used in drug delivery.

2. Results and Discussion

3.1 Noncovalent functionalization

Hydroxyurea, as shown in Fig.1, is non–planar drug with OH, NH_2, CO and NH groups. The γ-Fe_2O_3 nanoparticle was modeled using $Fe_6(OH)_{18}(H_2O)_6$ ring clusters of six-edge sharing octahead joining via 12 OH groups [25]. Figure 1 shows the optimized structures of the γ-Fe_2O_3 nanoparticle (MNP) and hydroxyurea (HU) in the solution phase.

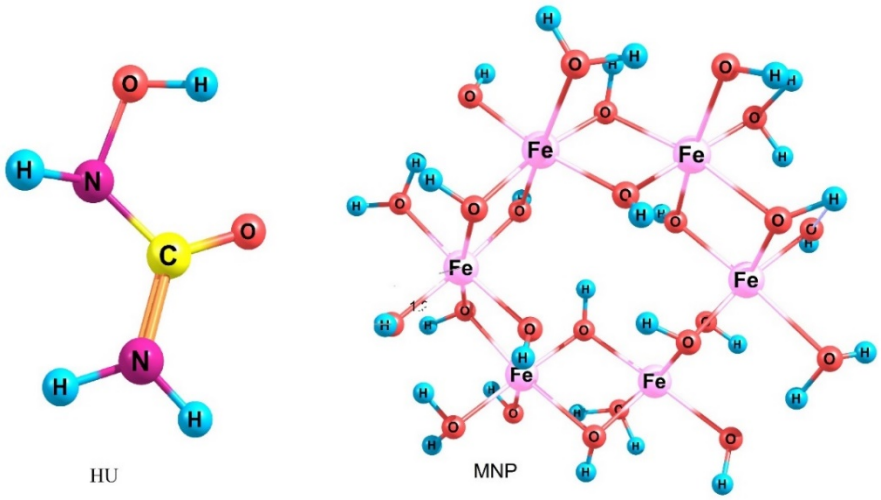

Figure 1. Optimized structures of HU and MNP.

The interaction between HU and MNP via the CO(MNP/HU1), NH_2(MNP/HU2), OH (MNP/ HU3) and NH(MNP/HU4) groups was considered in the gas phase and aqueous solution. These four configurations have been shown in Fig. 2. Hydrogen bond plays an important role in these configurations. The length of hydrogen bond (HB) in MNP/HU1-4 is 1.58-1.78 Aº (Fig.2).

Table 1 shows the salvation energies of HU, MNP and MNP/ HU 1-4. The binding energies (ΔE) of HU to MNP have been calculated in the gas phase and aqueous solution using the following equation:

$$\Delta E = E_{MNP/HU\,1\text{–}4} - (E_{MNP} + E_{HU}) \quad (1)$$

Table 1. Solvation and binding energies of different configurations (kJ mol^{-1}).

Species	Solvation energy	Binding energy	Binding energy
HU	-34.74	Solution	Gas
MNP	-126.25	phase	phase
MNP/HU1	-161.97	-29.34	-28.35
MNP/HU2	-154.13	-35.64	-42.49
MNP/HU3	-150.12	-49.58	-60.45
MNP/HU4	-146.57	-20.52	-34.94

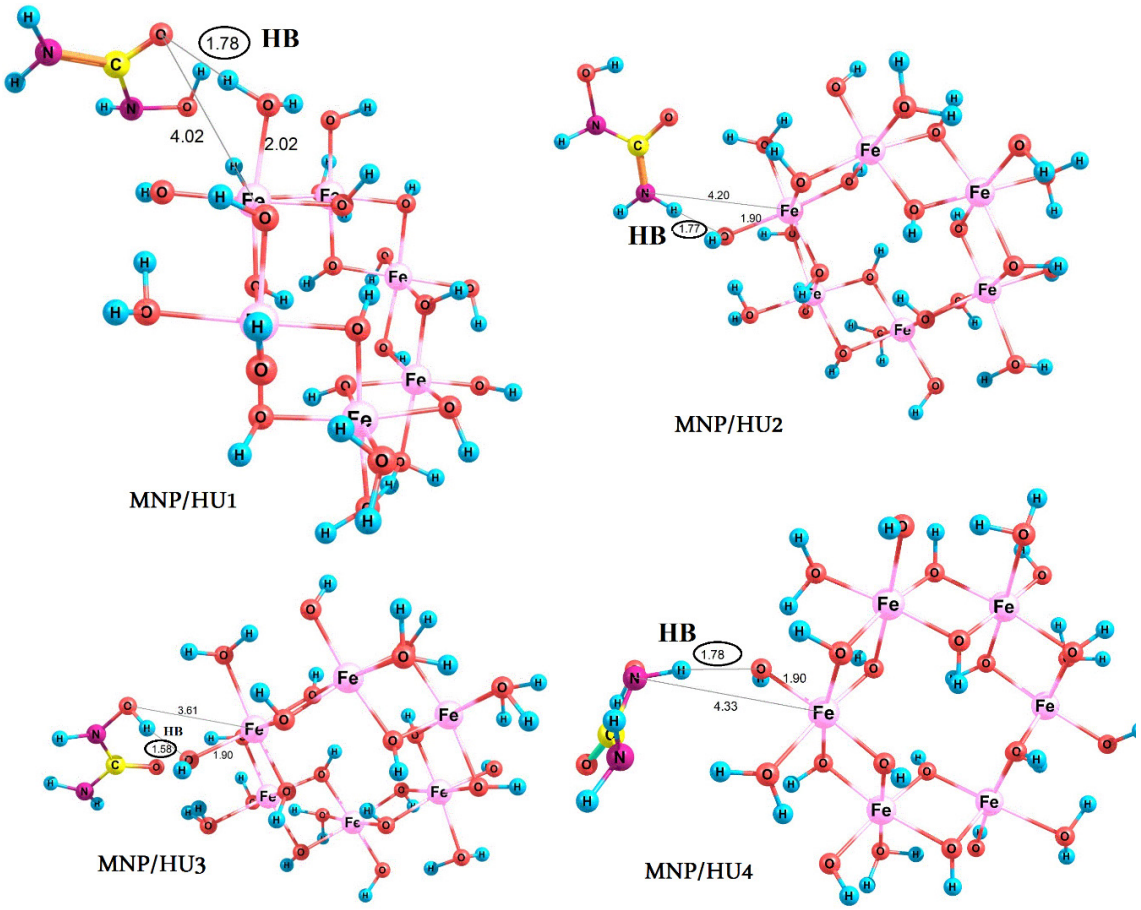

Figure 2. Optimized structures of MNP/HU1-4 (The length of the hydrogen bond is shown next to the symbol HB).

Table 2. Quantum molecular descriptors(eV) and binding energies(kJ mol^{-1})

Species	E_{HOMO}	E_{LUMO}	E_g	η	ω
	Solution phase (water)				
HU	-6.52	0.84	7.37	3.68	1.09
MNP	-5.58	-4.48	1.10	0.55	22.95
MNP/HU1	-5.53	-4.40	1.13	0.57	21.71
MNP/HU2	-5.f62	-4.51	1.11	0.56	23.06
MNP/HU3	-5.64	-4.53	1.11	0.56	23.28
MNP/HU4	-5.63	-4.53	1.11	0.55	23.33
	Gas phase				
HU	-6.44	0.70	7.14	3.57	1.15
MNP	-5.41	-4.36	1.05	0.53	22.68
MNP/HU1	-5.18	-4.13	1.04	0.52	20.76
MNP/HU2	-5.46	-4.39	1.07	0.54	22.60
MNP/HU3	-5.28	-4.26	1.01	0.51	22.41
MNP/HU4	-5.51	-4.45	1.06	0.53	23.49

The results of calculated solvation energies showed that the solubility of the HU increases in the presence of MNP. The binding energies of MNP/HU1- 4 are negative in the gas phase and aqueous solution showing HU is stabilized by MNP and the MNP/HU3 is the most stable configuration.

Quantum molecular descriptors, such as hardness and electrophilicity, play a key role in chemistry because they are used to describe chemical reactivity and stability. The resistance of a molecule to the change of its electronic structure can be expressed by global hardness (η). (Equation2).

Lower η can reduce the reactivity of the molecule and increase the stability.

$$\eta = (I - A)/2 \qquad (2)$$

where, $I = -E_{HOMO}$ is the ionization potential and $A = -E_{LUMO}$ is the electron affinity of the particle. The electrophilicity index (ω) is defined by Parr as follows [26]:

$$\omega = (I + A)^2 / 4\eta \qquad (3)$$

The quantum molecular descriptors for HU, MNP and MNP/HU1-4 are given for both gas and solution phases in Table 2, in which Eg has also been calculated (energy level difference between HOMO and LUMO) to determine a more stable configuration.

As the data in Table 1 indicate, η and Eg of HU is greater than MNP / HU1-4. These results showed that the reactivity of HU can increase in the presence of MNP. Here, HU acts as an electron acceptor because ω of HU increases in this case.

3.2 Covalent Functionalization

To study covalent functionalization in aqueous solution, we first examined MNP/HU2-4 configurations, where the hydroxyl and amine groups attack the Fe atom to transfer its proton to surface OH group of MNP. Scheme 1 is proposed for the mechanism of covalent bond formation between HU and MNP, where the MNP/HU2-4 configurations are converted to MNPHU2-4/H_2O by losing H_2O.

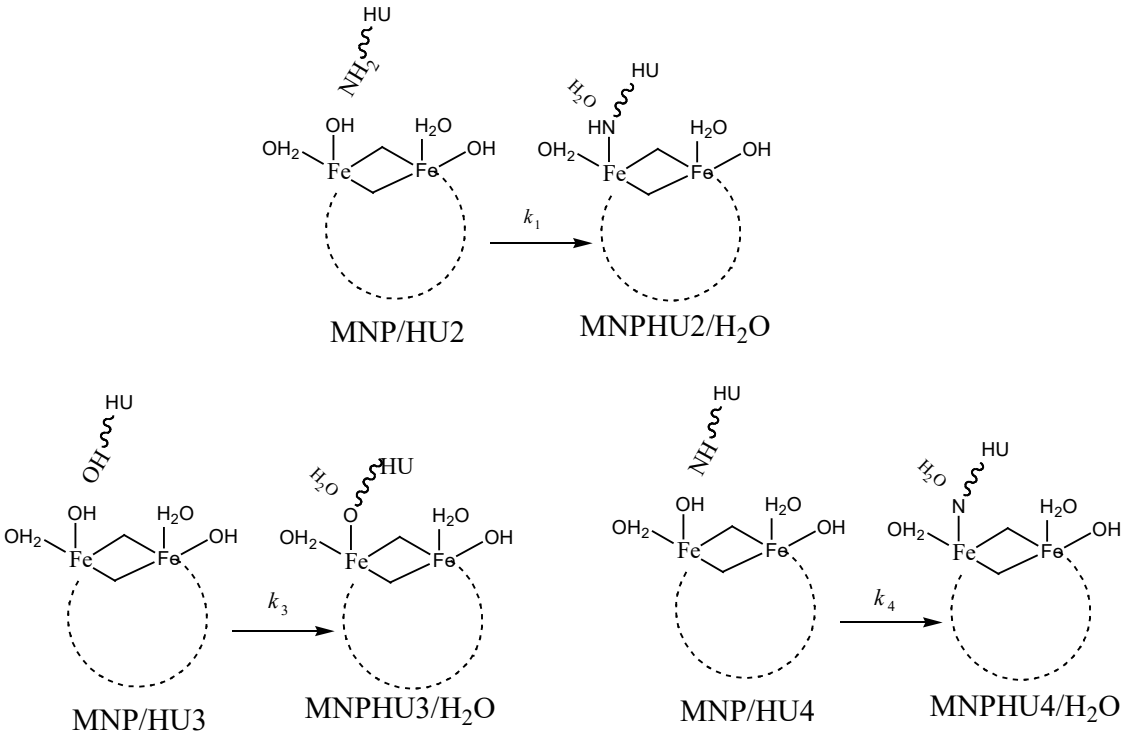

Scheme 1. k_2 – k_4 Mechanisms.

In this Scheme, the OH group on the surface of $Fe_6(OH)_{18}(H_2O)_6$ is substituted by the NH(O,N) of the drug HU to form MNPHU2(3,4) /H_2O. Fig. 3 shows the optimized structures of the MNPHU2-4/H_2O products. The transition state of the k_2 step was optimized using the MNP/HU2 reactant and the MNPHU2/H_2O product (called TS_{k2}; Fig 4). Figs. 3-4 show the bond lengths for all mechanisms.

The relative energies of optimized structures in all pathway were calculated with respect to electrical energy (E), enthalpy (H) and free gas (G) reactors at zero, as shown in Table 3. The activation energy (E_a), the activation enthalpy ($\Delta H^{\ddagger}$) and the activation Gibbs free energy ($\Delta G^{\ddagger}$) for the k_2 mechanism are equal to 52.50 kJ mol^{-1}, 53.81 kJ mol^{-1} and 64.57 kJ mol^{-1}, respectively (Table 3).

As for the k_2 step, we optimized the transition state of the k3 (k4) step (called $TS_{k3(k4)}$; Fig 4). According to Table 3, E_a, $\Delta H^{\ddagger}$ and $\Delta G^{\ddagger}$ are equal to 98.68 kJ mol^{-1}, 99.48 kJ mol^{-1} and 111.66 kJ mol^{-1} (56.17 kJ mol^{-1}, 57.48 kJ mol^{-1} and 65.59 kJ mol^{-1}) for the k_3 (k_4) step, respectively.

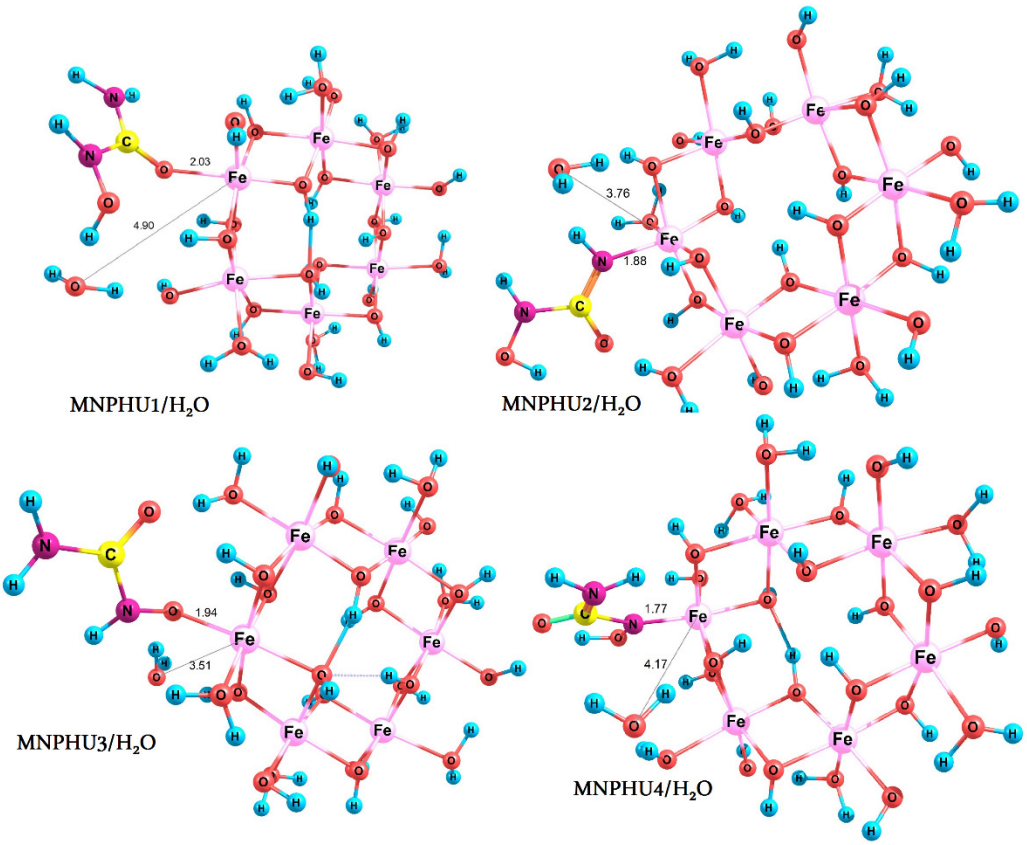

Figure 3. Optimized structures of MNPHU1-4/H_2O.

Table 3. Relative energies (kJ mol^{-1}) in k_1-k_4 mechanisms for different species.

Species	ΔE	ΔH	ΔG
		***k*₁ mechanism**	
MNP/HU1	0.00	0.00	0.00
TS_{k1}	48.88	49.31	57.70
MNPHU1/H_2O	-21.54	-24.01	-17.51
		*k*₂ mehanism	
MNP/HU2	0.00	0.00	0.00
TS_{k2}	52.50	53.81	64.57
MNPHU2/H_2O	13.93	12.68	24.34
		*k*₃ mehanism	
MNP/HU3	0.00	0.00	0.00
TS_{k3}	98.68	99.48	111.66
MNPHU3/H_2O	-50.32	-53.26	-45.15
		*k*₄ mehanism	
MNP/HU4	0.00	0.00	0.00
TS_{k4}	56.17	57.48	65.59
MNPHU4/H_2O	-101.88	-104.24	-92.19

In Scheme 2, the covalent functionalization of HU on MNP was examined in other reaction. H_2O of $Fe_6(OH)_{18}(H_2O)_6$ is substituted by the C=O group of HU to generate the MNPHU1/H_2O product. Fig. 3 shows the optimized structures of the MNPHU1/H_2O product. Using MNP/HU1 and MNPHU1/H_2O, the transition state for the k_1 step has been obtained (called TS_{k1}; Fig. 4). For this step, E_a, $\Delta H^{\ddagger}$ and $\Delta G^{\ddagger}$ are equal to 48.88 kJ mol^{-1}, 49.31 kJ mol^{-1} and 57.70 kJ mol^{-1}, respectively (Table 3).

The activation energy for the k_1 mechanism is lower than that of the k_2, k_3 and k_4 mechanisms, which are equal to 3.62 kJ mol^{-1}, 49.8 kJ mol^{-1} and 7.29 kJ mol^{-1}, respectively. As can be seen (Table 3), the third reaction (k3 mechanism) has high barrier energy and does not occur at room temperature. The second reaction (k2

mechanism) is nonspontaneous and endothermic. The first and fourth reactions are spontaneous and exothermic and have approximately the same activation energy but MNPHU4/H_2O product (k4 mechanism) is more stable than the MNPHU1/H_2O product (k1 mechanism), therefore, the k4 mechanism is the most appropriate pathway for covalent functionalization.

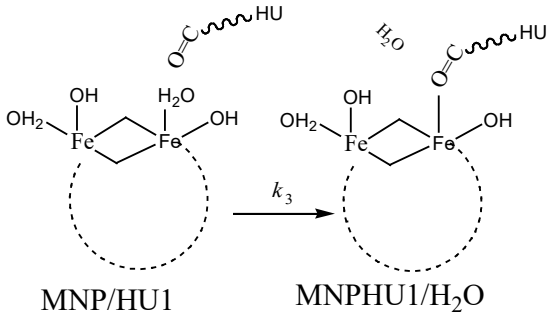

Scheme 2. k_1 Mechanism.

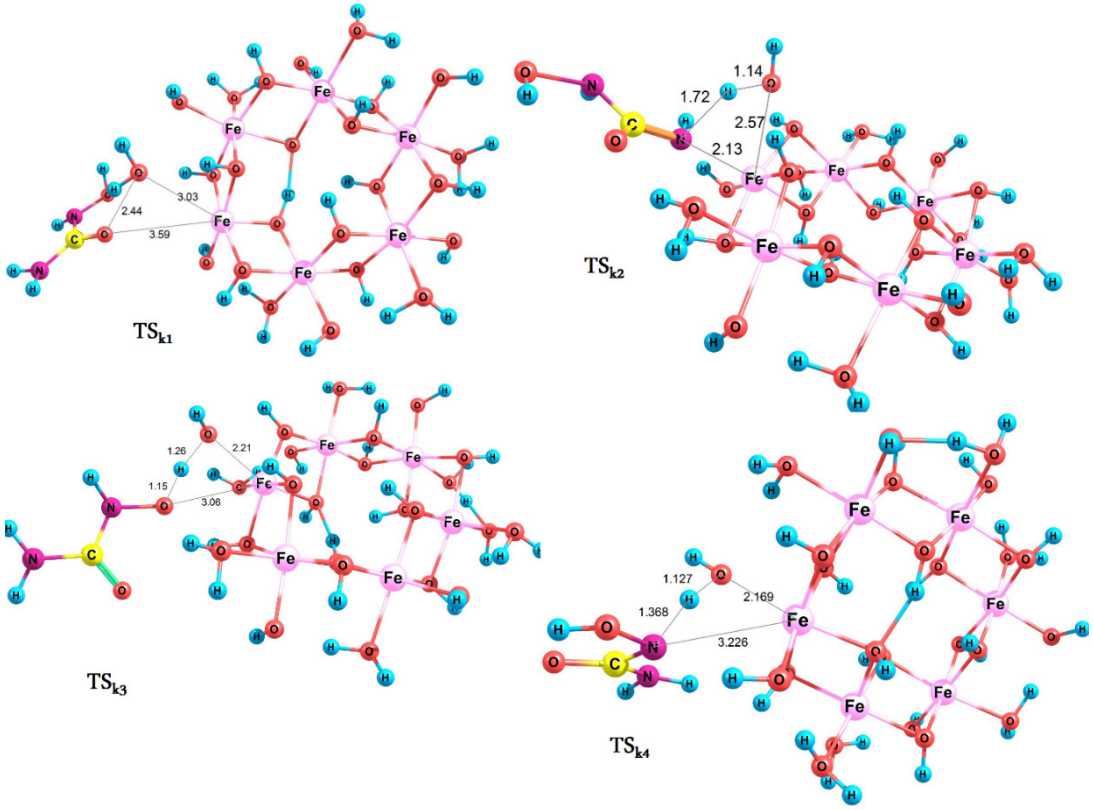

Figure 4. Optimized structures of TS_{k1-4}.

3. Material and Methods

All calculations were performed with B3LYP [27-29] a hybrid functional level used with the GAUSSIAN09 package [30]. It can be considered an improved method for calculating large molecules. The 6-31 G(d, p) basis set was used for all atoms, except Fe, where the LANL2DZ basis set was used with the effective core potential (ECP) function.

In chemistry, solvents are essential for the consideration of chemical processes [31,35]. The polarizable continuum model (PCM) is a commonly used method in computational chemistry to model the effects of solvent. In this study, aqueous solution was considered, because H2O is the major solvent in the human body. All degrees of freedom were optimized for all species [36-37]. The transition states were confirmed to have only one imaginary frequency of the Hessian. In addition, zero-point corrections were taken into account to obtain the activation energy.

4. Conclusions

In this study, four configurations for non-covalent functionalization of drug hydroxyurea

(HU) onto the γ-Fe_2O_3 nanoparticles (MNP) were examined in both gas and solution phases. MNPs were modeled using the ring clusters of $Fe_6(OH)_{18}(H_2O)_6$. The binding energies, calculated in the gas phase and aqueous solution for all the four configurations, were found to be negative, meaning that the configurations are energetically favorable. Since the global hardness and HOMO-LUMO energy gap of HU is higher than those of MNP/HU1-4, the reactivity of HU can increase in the presence of the γ-Fe_2O_3 nanoparticles. We also studied four configurations for covalent functionalization of the drug hydroxyurea (HU) loaded on MNP via the CO (k_1 mechanism), NH_2 (k_2 mechanism), OH (k_3 mechanism) and NH (k_4 mechanism) groups. The k_4 mechanism has been determined to be the most appropriate mechanism because it has low energy barrier and leads to the most stable product.

Acknowledgments

We thank the Research Center for Animal Development Applied Biology for allocation of computer time.

References and Notes

[1] Corot, C.; Robert, P.; Idée, J. M.; Port, M. *Adv. Drug Delivery Rev.* **2006**, *58*, 1471. [Crossref]

[2] Whitesides, G. M. *Nat. Biotechnol.* **2003**, *21*, 1161.

[3] Gupta, A. K.; Gupta, M. *Biomaterials* **2005**, *26*, 3995. [Crossref]

[4] Prijic, S.; Sersa, G. *Radiol. Oncol.* **2011**, *45*, 1. [Crossref]

[5] LaConte, L.; Nitin, N.; Bao, G. *Mater. Today* **2005**, *8*, 32. [Crossref]

[6] Hochepied, J.; Bonville, P.; Pileni, M. *J. Phys. Chem. B* **2000**, *104*, 905. [Crossref]

[7] Lübbe, A. S.; Bergemann, C.; Riess, H.; Schriever F.; Reichardt, P.; Possinger, K. *Cancer Res.* **1996**, *56*, 4686.

[8] Lübbe, A. S.; Alexiou, C.; Bergemann, C. *J. Surg. Res.* **2001**, *95*, 200. [Crosrref]

[9] Ferrari, M. *Nat. Rev. Cancer* **2005**, *5*, 161. [Crossref]

[10] Pankhurst, Q. A.; Connolly, J. Jones, S.; Dobson, J. *J. Phys. D: Appl. Phys.* **2003**, *36*, R167.

[11] Dobson, J. *Drug Dev. Res.* **2006**, *67*, 55. [Crossref]

[12] Senyei, A.; Widder. K.; Czerlinski, G. *J. Appl. Phys.* **1978**, *49*, 3578. [Crossref]

[13] Neuberger, T.; Schöpf, B.; Hofmann, H.; Hofmann, M.; Von Rechenberg, B. *J. Magn. Magn. Mater.* **2005**, *293*, 483. [Crossref]

[14] Yoo, J. W.; Doshi, N.; Mitragotri, S. *Adv. Drug Delivery Rev.* **2011**, *63*, 1247. [Crossref]

[15] Chacko, R. T.; Ventura, J.; Zhuang, J.; Thayumanavan, S. *Adv. Drug Delivery Rev.* **2012**, *64*, 836. [Crossref]

[16] Weissleder, R.; Stark, D. D.; Engelstad, B. L.; Bacon, B. R.; Compton, C. C.; White, D. L; et al. *Am. J. Roentgenol.* **1989**, *152*, 167. [Crossref]

[17] Figuerola, A.; Di Corato, R.; Manna, L.; Pellegrino, T. *Pharmacol. Res.* **2010**, *62*, 126. [Crossref]

[18] Mahmoudi, M.; Sant, S.; Wang, B.; Laurent, S.; Sen, T. *Adv. Drug Delivery Rev.* **2011**, *63*, 24. [Crossref]

[19] Tartaj, P.; Morales, M. P.; Veintemillas-Verdaguer, S.; González-Carreño, T.; Serna, C. J. *J. Phys. D: Appl. Phys.* **2003**, *36*, R182.

[20] Ito, A.; Shinkai, M.; Honda, H.; Kobayashi, T. *J. Biosci. Bioeng.* **2005**, *100*, 1. [Crossref]

[21] Marconato, L.; Bonfanti, U.; Fileccia, I. *J. Small Anim. Pract.* **2007**, *4*, 514. [Crossref]

[22] Liebelt, E. L.; Balk, S. J.; Faber, W.; Fisher, J. W.; Hughes, C. L.; Lanzkron, S. M.; *Birth Defects Res., Part B* **2007**, *80*, 259. [Crossref]

[23] Zheng, Y. B.; Kiraly, B.; Huang, T. J. *Nanomedicine* **2010**, *5*, 1309. [Crossref]

[24] Linko, V.; Ora, A.; Kostiainen, M. A. *Trends Biotechnol.* **2015**, *33*, 586. [Crossref]

[25] Jayarathne, L.; Ng, W. J.; Bandara, A.; Vitanage, M.; Dissanayake, C.; Weerasooriya, R. *Colloids Surf., A* **2012**, *403*, 96. [Crossref]

[26] Parr, R. G.; Szentpaly, L.; Liu, S. *J. Am. Chem. Soc.* **1999**, *121*, 1922. [Crossref]

[27] Becke, A. D. *Phys. Rev. A* **1988**, *38*, 3098. [Crossref]

[28] Becke, A. D. *J. Chem. Phys.* **1993**, *98*, 5648. [Crossref]

[29] Lee, C.; Yang, W.; Parr, R. G. *Phys. Rev. B* **1988**, *37*, 785. [Crossref]

[30] Frisch, M. J.; Trucks, G.; Schlegel, H. B.; Scuseria, G.; Robb, M.; Cheeseman, J. *Gaussian Inc Wallingford CT* **2009**, *27*, 34.

[31] Akbari, A.; Hoseinzade, F.; Morsali, A.; Beyramabadi, S. A. *Inorg. Chim. Acta* **2013**, *394*, 423. [Crossref]

[32] Morsali, A.; Hoseinzade, F.; Akbari, A.; Beyramabadi, S. A.; Ghiasi, R. *J. Solution Chem.* **2013**, *42*, 1902. [Crossref]

[33] Gharib, A.; Morsali, A.; Beyramabadi, S.; Chegini, H.; Ardabili, M. N. *Prog. React. Kinet. Mech.* **2014**, *39*, 354. [Crossref]

[34] Morsali, A. *Int. J. Chem. Kinet.* **2015**, *47*, 73 [Crossref]

[35] Ardabili, M. N.; Morsali, A.; Beyramabadi, S. A.; Chegini, H.; Gharib, A. *Res. Chem. Intermed.* **2015**, *41*, 5389. [Crossref]

[36] Cammi, R.; Tomasi, J. *J. Comput. Chem.* **1995**, *16*, 1449. [Crossref]

[37] Tomasi, J.; Persico, M. *Chem. Rev.* **1994**, *94*, 2027. [Crossref]